RSC Advances

PAPER

View Article Online
View Journal | View Issue

Cite this: *RSC Adv.*, 2021, **11**, 11529

Synthesis of zirconocene complexes and their use in slurry-phase polymerisation of ethylene†

Phakpoom Angpanitcharoen, Jessica V. Lamb, Jean-Charles Buffet, Zoë R. Turner and Dermot O'Hare *

A new family of zirconocene complexes of the type $(^{3\text{-R}}\text{Ind}^{\#})_2ZrX_2$ (where $\text{Ind}^{\#} = C_6Me_5H$ and R = Me, Et and Ph) have been synthesised and fully characterised. Six new crystal structures have been reported (*meso*-$(^{3\text{-Et}}\text{Ind}^{\#})_2ZrBr_2$, *rac*-$(^{3\text{-Et}}\text{Ind}^{\#})_2ZrCl_2$, *rac*-$(^{3\text{-Et}}\text{Ind}^{\#})_2Zr(CH_2Ph)_2$, *meso*-$(^{3\text{-Et}}\text{Ind}^{\#})_2Zr(CH_2Ph)_2$, *meso*-$(^{3\text{-Me}}\text{Ind}^{\#})_2ZrBr_2$ and *meso*-$(^{3\text{-Me}}\text{Ind}^{\#})_2Zr(CH_2Ph)_2$). The complexes were studied for slurry-phase ethylene polymerisation when immobilised on solid polymethylaluminoxane (sMAO). Variation in the initiation group was found to have greater influence over polymerisation activity for *meso*-catalysts than *rac*-catalysts, with *meso*-alkyl catalysts showing higher polymerisation activities than *meso*-halide. Below 70 °C, polymerisation activity follows the order sMAO-*meso*-$(^{3\text{-Et}}\text{Ind}^{\#})_2Zr(CH_2Ph)_2$, sMAO-*meso*-$(^{3\text{-Et}}\text{Ind}^{\#})_2ZrCl_2$ and sMAO-*meso*-$(^{3\text{-Et}}\text{Ind}^{\#})_2ZrBr_2$ (activities of 657, 561, and 452 kg_{PE} mol_M^{-1} h^{-1} bar^{-1}, respectively). sMAO-*meso*-$(^{3\text{-Et}}\text{Ind}^{\#})_2ZrBr_2$ produces HDPE with the highest molecular weight, followed by sMAO-*meso*-$(^{3\text{-Et}}\text{Ind}^{\#})_2ZrCl_2$ and sMAO-*meso*-$(^{3\text{-Et}}\text{Ind}^{\#})_2Zr(CH_2Ph)_2$ (M_w of 503, 406, and 345 kg mol^{-1}, respectively, at 50 °C). sMAO-*meso*-$(^{3\text{-Me}}\text{Ind}^{\#})_2ZrBr_2$ produced HDPE with almost identical molecular weights to sMAO-*meso*-$(^{3\text{-Et}}\text{Ind}^{\#})_2ZrCl_2$ (395 kg mol^{-1} at 50 °C).

Received 10th March 2021
Accepted 11th March 2021

DOI: 10.1039/d1ra01912k

rsc.li/rsc-advances

Introduction

Group 4 metallocenes are generally defined as d^0, pseudo-tetrahedral organometallic compounds in which the transition metal atom bears two η^5-cyclopentadienyl-based ligands and two σ-ligands.[1] Upon the activation of group 4 metallocenes by co-catalysts (*e.g.* MAO),[2] the resulting highly electrophilic alkyl metallocene cations, stabilised by non-nucleophilic, very weakly coordinating anions, are known to be the active species for α-olefin polymerisation.[3–5] The stability of the cationic intermediate and the electron density, accessibility and geometry of the active site, all of which are influenced by ligand structure, are believed to be the main influencing factors towards reactivity and stereospecificity.[6]

The discovery of 'single-site' metallocene-based catalysts has revived α-olefin polymerisation chemistry as these catalyst systems enable the production of (co)polyolefins with tuneable molecular structures, stereochemistries and molecular weight distributions (MWD, M_w/M_n).[7–14] Self-immobilisation of catalyst and co-catalysts for olefin polymerisation has shown that the high excess of MAO can reduced by more than 90%.[15] Yet these catalysts are rarely used for industrial processes, with a few exceptions including Dowlex (Dow) and Sclairtech (Nova Chem. Corp.); due to the incompatibility with the existing gas or slurry phase olefin polymerisation processes. By immobilising metallocene catalysts onto support materials, the processability problem is solved and the advantages of metallocene catalysts, including narrow MWD, high activity, and precise control over polymer microstructure, are preserved to a great extent. Supporting metallocene complexes also allows for the reduction of the ratio of MAO to metallocene,[16] and have an dramatic effect on the tacticity when polymerising α-olefins.[8] Many materials were tested as olefin polymerisation supports including inorganic solids such as silica,[17] silicate clays,[18] $MgCl_2$,[19] and polymeric aluminoxanes.[20] Various functionalised polymers have also been investigated as supports. Silica is the most commonly used support for heterogeneous metallocene catalysts. Pre-contacting the silica surface with MAO was reported to increase catalyst loadings.[21–24] The use of layered double hydroxides (LDHs), a class of anionic clays consisting of positively charged Brucite-like layers with weakly bound anions intercalated between them, as catalyst supports for olefin polymerisation has been recently reported by the O'Hare group.[25–27] Heat treatment of MAO for a prolonged period was reported to increase polymerisation activity of up to 25%. This is believed to be caused by the aggregation of MAO to form larger particles which are insoluble in hydrocarbon solvents. This insoluble 'solid MAO' can act simultaneously as both co-catalyst and support in slurry phase ethylene polymerisation.[28,29]

Chemistry Research Laboratory, Department of Chemistry, University of Oxford, OX1 3TA, UK. E-mail: Dermot.ohare@chem.ox.ac.uk

† Electronic supplementary information (ESI) available: NMR spectroscopy, X-ray crystallography, polymerisation data. CCDC 2058030–2058035, 2058038 and 2058039. For ESI and crystallographic data in CIF or other electronic format see DOI: 10.1039/d1ra01912k

Results and discussion

Synthesis of $(^{3\text{-R}}\text{Ind}^{\#})_2ZrX_2$ (R = Me, Et or Ph; X= Cl, Br or CH_2Ph)

$^{3\text{-Ph}}\text{Ind}^{\#}\text{Li}$ was synthesised according to a modified literature procedure (Fig. S1–S10†).[30] Two equivalents $^{3\text{-Ph}}\text{Ind}^{\#}\text{Li}$ were reacted with one equivalent of $ZrCl_4$ to afford a 50 : 50 mixture of *rac*- and *meso*-$(^{3\text{-Ph}}\text{Ind}^{\#})_2ZrCl_2$ (**1**) as an orange yellow solid in 45% yield (Scheme 1). The two sets of resonances corresponding to each isomer are indistinguishable in the ^{1}H NMR spectrum; resonances between 6.90 and 7.90 ppm correspond to the phenyl protons, while two singlets at 5.86 and 6.52 ppm correspond to the cyclopentadienyl protons and singlets between 1.60 and 2.80 ppm correspond to the methyl groups on the indenyl rings (Fig. S11†).

$^{3\text{-Et}}\text{Ind}^{\#}\text{Li}$ was synthesised according to a previously reported procedure.[30] Two equivalents of $^{3\text{-Et}}\text{Ind}^{\#}\text{Li}$ were reacted with one equivalent $ZrBr_4$ to afford an orange solid comprising of a 40 : 60 mixture of *rac*- and *meso*-$(^{3\text{-Et}}\text{Ind}^{\#})_2ZrBr_2$ after work-up. Recrystallisation of the isomeric mixture yielded *meso*-$(^{3\text{-Et}}\text{Ind}^{\#})_2ZrBr_2$ (***meso*-2**) as orange crystals in 6% yield. Similar to **1**, ***meso*-2** shows diagnostic resonances corresponding to the cyclopentadienyl proton and methyl groups of the indenyl rings. ***meso*-2** also shows two doublet of quartets at 2.69 and 3.22 ppm and a triplet at 1.05 ppm corresponding to the diastereotopic methylene and methyl protons of the ethyl groups respectively (Fig. S13†).

rac-$(^{3\text{-Et}}\text{Ind}^{\#})_2ZrCl_2$ (***rac*-3**) and *meso*-$(^{3\text{-Et}}\text{Ind}^{\#})_2ZrCl_2$ (***meso*-3**) were prepared according to a literature procedure.[30] They were reacted with two equivalents KCH_2Ph to afford *rac*-$(^{3\text{-Et}}\text{Ind}^{\#})_2Zr(CH_2Ph)_2$ (***rac*-4**) and *meso*-$(^{3\text{-Et}}\text{Ind}^{\#})_2Zr(CH_2Ph)_2$ (***meso*-4**) as a yellow solids, both in 93% yield after work-up. The C_2-symmetry of ***rac*-4** results in magnetically equivalent indenyl rings and benzyl groups, as evidenced in the ^{1}H NMR spectrum;

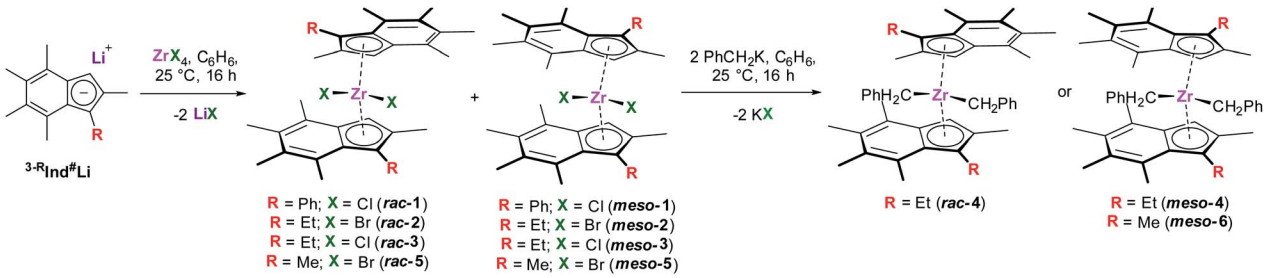

Scheme 1 Synthesis of *rac*-$(^{3\text{-Ph}}\text{Ind}^{\#})_2ZrCl_2$ (***rac*-1**), *meso*-$(^{3\text{-Ph}}\text{Ind}^{\#})_2ZrCl_2$ (***meso*-1**), *rac*-$(^{3\text{-Et}}\text{Ind}^{\#})_2ZrBr_2$ (***rac*-2**), *meso*-$(^{3\text{-Et}}\text{Ind}^{\#})_2ZrBr_2$ (***meso*-2**), *rac*-$(^{3\text{-Et}}\text{Ind}^{\#})_2ZrCl_2$ (***rac*-3**), *meso*-$(^{3\text{-Et}}\text{Ind}^{\#})_2ZrCl_2$ (***meso*-3**), *rac*-$(^{3\text{-Et}}\text{Ind}^{\#})_2Zr(CH_2Ph)_2$ (***rac*-4**), *meso*-$(^{3\text{-Et}}\text{Ind}^{\#})_2Zr(CH_2Ph)_2$ (***meso*-4**), *rac*-$(^{3\text{-Me}}\text{Ind}^{\#})_2ZrBr_2$ (***rac*-5**), *meso*-$(^{3\text{-Me}}\text{Ind}^{\#})_2ZrBr_2$ (***meso*-5**), and *meso*-$(^{3\text{-Me}}\text{Ind}^{\#})_2Zr(CH_2Ph)_2$ (***meso*-6**).

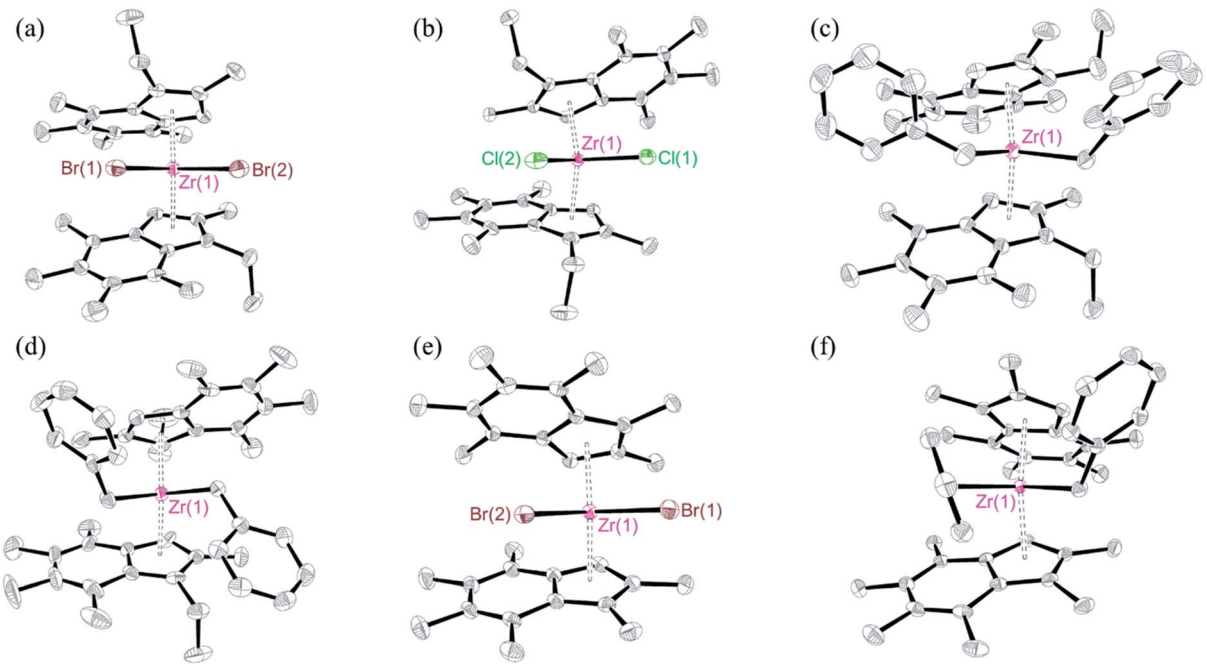

Fig. 1 Molecular structure of (a) *meso*-$(^{3\text{-Et}}\text{Ind}^{\#})_2ZrBr_2$ (***meso*-2**), (b) *rac*-$(^{3\text{-Et}}\text{Ind}^{\#})_2ZrCl_2$ (***rac*-3**), (c) *meso*-$(^{3\text{-Et}}\text{Ind}^{\#})_2Zr(CH_2Ph)_2$ (***meso*-4**), (d) *rac*-$(^{3\text{-Et}}\text{Ind}^{\#})_2Zr(CH_2Ph)_2$ (***rac*-4**), (e) *meso*-$(^{3\text{-Me}}\text{Ind}^{\#})_2ZrBr_2$ (***meso*-5**), and (f) *meso*-$(^{3\text{-Me}}\text{Ind}^{\#})_2Zr(CH_2Ph)_2$ (***meso*-6**). Hydrogen atoms omitted for clarity, ellipsoids drawn at 50% probability.

the phenyl protons are seen as a doublet, doublet of doublets, and triplet at 6.62, 7.08, and 6.80 ppm, respectively, while two doublets at 0.67 and 0.87 ppm correspond to the diastereotopic benzylic protons (Fig. S15†). Similar to *meso*-^{Me_2}SB($^{3\text{-Et}}$I*)Zr(CH_2Ph)$_2$,[31] the symmetry of ***meso*-4** results in magnetically inequivalent benzyl groups in the ^{1}H NMR spectrum; the *ortho*, *meta*, *para*, and benzylic protons of one benzyl group are observed as a doublet at 6.46 ppm, a doublet of doublets at 7.04 ppm, a triplet at 6.75 ppm, and a singlet at 0.24 ppm, while for the other benzyl group they appear at 6.58, 7.06, 6.79, and 0.79 ppm (Fig. S17†). $^{3\text{-Me}}$Ind$^{\#}$Li was synthesised according to a previously reported procedure.[32] Two equivalents $^{3\text{-Me}}$Ind$^{\#}$Li were reacted with one equivalent $ZrBr_4$ to afford an orange solid comprising of a 20 : 80 mixture of *rac*- and *meso*-($^{3\text{-Me}}$Ind$^{\#}$)$_2$ZrBr$_2$, and impurities. Recrystallisation of the isomeric mixture in toluene at −30 °C yielded *meso*-($^{3\text{-Me}}$Ind$^{\#}$)$_2$ZrBr$_2$ (***meso*-5**) as orange crystals in 6% yield. The ^{1}H NMR spectrum of ***meso*-5** shows that the two indenyl rings are magnetically equivalent, with diagnostic resonances corresponding to the cyclopentadienyl protons and indenyl methyl groups (Fig. S19†). One equivalent ***meso*-5** was further reacted with two equivalents of KCH_2Ph to afford *meso*-($^{3\text{-Me}}$Ind$^{\#}$)$_2$Zr(CH_2Ph)$_2$ (***meso*-6**) as a yellow solid in 88% yield. Similar to ***meso*-4**, the C_s-symmetry of ***meso*-6** results in magnetically inequivalent benzyl groups in the ^{1}H NMR spectrum (Fig. S21†).

Orange crystals of ***meso*-2**, ***rac*-4**, and ***meso*-4** were grown from pentane at room temperature, while crystals of ***rac*-3**, ***meso*-5** and ***meso*-6** were grown from a toluene solution at −30 °C and room temperature. The solid-state molecular structures are depicted in Fig. 1, with selected bond lengths and angles presented in Table 1.

For ***meso*-2**, the average Zr–Br bond length (2.598 Å) and Zr–Cp_{cent} distance (2.243 Å) are within the range of those reported for other unbridged dibromobisindenyl zirconocene complexes.[16–18] The ring tilt angle (α) (52.44°) and angle about the metal centre (δ) (131.93) are similar to *meso*-($^{3\text{-Me}}$Ind$^{\#}$)$_2$ZrCl$_2$ (53.28° and 132.02°, respectively).[32] The torsion angle (TA) measures the twist of the two indenyl rings relative to one another (Fig. S23†). The introduction of ethyl groups causes increased steric strain, resulting in ***meso*-2** adopting 'gauche' conformation, which is reflected in the TA angle of 81.49° compared to 37.16° for *meso*-($^{3\text{-Me}}$Ind$^{\#}$)$_2$ZrCl$_2$.[32]

The average Zr–Cl bond length and Zr–Cp_{cent} distance of ***rac*-3** (2.435 and 2.241 Å) are in good agreement with the 3-methyl analogue *rac*-($^{3\text{-Me}}$Ind$^{\#}$)$_2$ZrCl$_2$ (2.421 and 2.228 Å).[32] The α and δ values (Fig. S23†) of ***rac*-3** (51.72° and 132.44°) are comparable to *rac*-($^{3\text{-Me}}$Ind$^{\#}$)$_2$ZrCl$_2$ (51.58° and 133.59°) and *rac*-($^{3\text{-Et}}$Ind$^{\#}$)$_2$HfCl$_2$ (51.80° and 132.56°), as are the torsion angles (173.14, 171.31, and 173.01°, respectively), implying that the introduction of 3-ethyl groups has little-to-no impact on the molecular frameworks. Structure comparisons of ***rac*-3** with the unmethylated analog, *rac*-($^{1\text{-Et}}$Ind)$_2$ZrCl$_2$, show similar average Zr–Cl bond lengths (2.435 and 2.442 Å) and Zr–Cp_{cent} distances (2.241 and 2.233 Å).[33] The α and δ values for *rac*-3 (51.72° and 132.44°) are slightly larger than for *rac*-($^{1\text{-Et}}$Ind)$_2$ZrCl$_2$ (49.22° and 131.98°). However, the TA value for ***rac*-3** (173.14°) is significantly larger than for *rac*-($^{1\text{-Et}}$Ind)$_2$ZrCl$_2$ (120.02°) due to the increased sterics of methylation. For ***meso*-4**, the average Zr–CH_2Ph bond length (2.318 Å) is similar to ***rac*-4** (2.303 Å) and the hexamethylated analogue *rac*-($^{3\text{-Me}}$Ind$^{\#}$)$_2$Zr(CH_2Ph)$_2$ (2.320 Å),[32] and is slightly longer than ($^{4,7\text{-F}}$Ind)$_2$Zr(CH_2Ph)$_2$ (2.294 Å).[34] Similar to ***meso*-2**, ***meso*-4** has a TA value of 102.95°, adopting 'gauche' conformation to minimise the steric clash between the ethyl and benzyl groups. The average Zr–Br bond length and Zr–Cp_{cent} distances of ***meso*-5** (2.594 and 2.251 Å) are similar to ***meso*-2** (2.598 and 2.243 Å). The α value for ***meso*-5** (54.35°) is slightly larger than *meso*-($^{3\text{-Me}}$Ind$^{\#}$)$_2$ZrCl$_2$ (53.28°) due to the larger Br ligands.[32] The TA value of 35.46° for ***meso*-5** is comparable to *meso*-($^{3\text{-Me}}$Ind$^{\#}$)$_2$ZrCl$_2$ (37.16°),[32] however, is significantly less than ***meso*-2** (81.49°) due to the decrease in steric strain on exchanging ethyl for methyl. For ***meso*-6**, the average Zr–CH_2Ph bond length (2.322 Å) is comparable to ***rac*-4** (2.302 Å) and *rac*-($^{3\text{-Me}}$Ind$^{\#}$)$_2$Zr(CH_2Ph) (2.320 Å).[32] However, comparisons between the α values of ***meso*-6** and ***rac*-4** are challenging because the complexes adopt different conformations, reflected in the TA values of 112.56° and 157.30°, in order to minimise the steric interactions between the indenyl and benzyl ligands.

Table 1 Selected bond lengths (Å) and angles (°) for *meso*-($^{3\text{-Et}}$Ind$^{\#}$)$_2$ZrBr$_2$ (***meso*-2**), *rac*-($^{3\text{-Et}}$Ind$^{\#}$)$_2$ZrCl$_2$ (***rac*-3**), (*meso*-($^{3\text{-Et}}$Ind$^{\#}$)$_2$Zr(CH_2Ph)$_2$ (***meso*-4**), *rac*-($^{3\text{-Et}}$Ind$^{\#}$)$_2$Zr(CH_2Ph)$_2$ (***rac*-4**), *meso*-($^{3\text{-Me}}$Ind$^{\#}$)$_2$ZrBr$_2$ (***meso*-5**), and *meso*-($^{3\text{-Me}}$Ind$^{\#}$)$_2$Zr(CH_2Ph)$_2$ (***meso*-6**)[a]

	Complex	Zr-X	Zr-Cp_{cent}	α	δ	TA
***meso*-2**	*meso*-($^{3\text{-Et}}$Ind$^{\#}$)$_2$ZrBr$_2$	2.6041(5)	2.2425(11)	52.44(14)	131.93(4)	81.49
		2.5927(5)	2.2430(11)			
***rac*-3**	*rac*-($^{3\text{-Et}}$Ind$^{\#}$)$_2$ZrCl$_2$	2.4183(6)	2.2453(8)	51.72(10)	132.44(3)	173.14
		2.4514(6)	2.2374(8)			
***meso*-4**	*meso*-($^{3\text{-Et}}$Ind$^{\#}$)$_2$Zr(CH_2Ph)$_2$	2.307(2)	2.3045(8)	51.80(11)	132.99(3)	102.95
		2.3284(19)	2.2666(9)			
***rac*-4**	*rac*-($^{3\text{-Et}}$Ind$^{\#}$)$_2$Zr(CH_2Ph)$_2$	2.307(7)	2.322(3)	51.9(4)	133.63(11)	157.30
		2.299(7)	2.281(3)			
***meso*-5**	*meso*-($^{3\text{-Me}}$Ind$^{\#}$)$_2$ZrBr$_2$	2.6133(4)	2.2500(10)	54.35(13)	133.62(4)	35.46
		2.5745(4)	2.2525(10)			
***meso*-6**	*meso*-($^{3\text{-Me}}$Ind$^{\#}$)$_2$Zr(CH_2Ph)$_2$	2.3302(18)	2.2763(9)	53.66(10)	133.92(3)	112.56
		2.3132(18)	2.3419(10)			

[a] X = Br, Cl or CH_2Ph; α, δ and TA: crystallographic parameters are defining in Fig. S23.

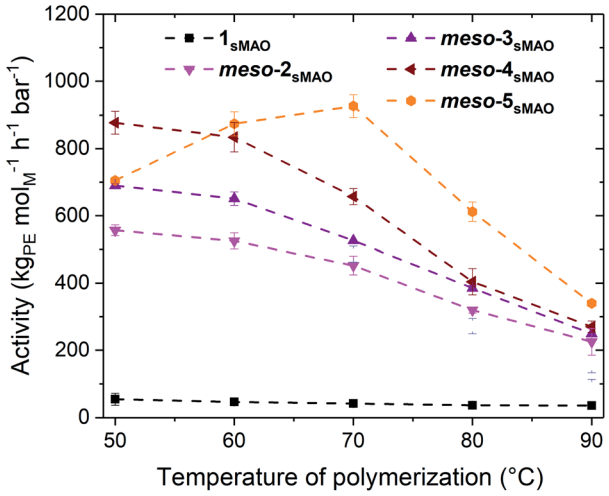

Fig. 2 Polymerisation activity as a function of temperature of polymerisation using sMAO supported 50 : 50 *rac*- and *meso*-($^{3\text{-Ph}}$Ind$^{\#}$)$_2$ZrCl$_2$ (**1**$_{sMAO}$; black square), *meso*-($^{3\text{-Et}}$Ind$^{\#}$)$_2$ZrBr$_2$ (***meso*-2**$_{sMAO}$; pink down triangle), *meso*-($^{3\text{-Et}}$Ind$^{\#}$)$_2$ZrCl$_2$ (***meso*-3**$_{sMAO}$; purple triangle), *meso*-($^{3\text{-Et}}$Ind$^{\#}$)$_2$Zr(CH$_2$Ph)$_2$ (***meso*-4**$_{sMAO}$; brown right triangle), and *meso*-($^{3\text{-Me}}$Ind$^{\#}$)$_2$ZrBr$_2$ (***meso*-5**$_{sMAO}$; orange hexagon). Polymerisation conditions: ethylene (2 bar), pre-catalyst (10 mg), hexane (50 mL), [Al$_{sMAO}$]$_0$/[Zr]$_0$ = 200, TiBA (1000 eq.), and 30 minutes.

Slurry-phase ethylene polymerisation

A 50 : 50 mixture of *rac*- and *meso*-($^{3\text{-Ph}}$Ind$^{\#}$)ZrCl$_2$ (**1**), *meso*-($^{3\text{-Et}}$Ind$^{\#}$)$_2$ZrBr$_2$ (***meso*-2**), *rac*-($^{3\text{-Et}}$Ind$^{\#}$)$_2$ZrCl$_2$ (***rac*-3**), *meso*-($^{3\text{-Et}}$Ind$^{\#}$)$_2$ZrCl$_2$ (***meso*-3**), *rac*-($^{3\text{-Et}}$Ind$^{\#}$)$_2$Zr(CH$_2$Ph)$_2$ (***rac*-4**), *meso*-($^{3\text{-Et}}$Ind$^{\#}$)$_2$Zr(CH$_2$Ph)$_2$ (***meso*-4**) *meso*-($^{3\text{-Me}}$Ind$^{\#}$)$_2$ZrBr$_2$ (***meso*-5**$_{sMAO}$) were immobilised on solid polymethylaluminoxane (sMAO)[28,29,35] according to a literature procedure with an initial aluminium to zirconium ([Al$_{sMAO}$]$_0$/[Zr]$_0$) loading of 200.[30] Slurry-phase ethylene polymerisations were conducted in 150 mL ampoules with 50 mL hexane, 10 mg pre-catalyst and 2 bar ethylene at 50–90 °C for 30 minutes with triisobutylaluminium (TiBA, Al(CH$_2$CH(CH$_3$)$_2$)$_3$) scavenger with [Al$_{scav}$]$_0$/[M]$_0$ of 1000 (Fig. 2).

1$_{sMAO}$ shows significantly lower polymerisation activities than ***rac*-3**$_{sMAO}$ and ***meso*-3**$_{sMAO}$, likely due to the large steric bulk of the phenyl groups. ***rac*-3**$_{sMAO}$ displays higher polymerisation activities than ***meso*-3**$_{sMAO}$ below 70 °C, and almost identical polymerisation activities above 70 °C, while ***rac*-4**$_{sMAO}$ and ***meso*-4**$_{sMAO}$ display similar polymerisation activities across the entire temperature range. ***rac*-3** shows significantly higher polymerisation activities when immobilised on sMAO compared to MAO modified silica (activities of 561 and approximately 75 kg$_{PE}$ mol$_M^{-1}$ h^{-1} bar^{-1} respectively at 70 °C).[30] ***rac*-3**$_{sMAO}$ and ***rac*-4**$_{sMAO}$ show lower polymerisation activities than the 3-methyl analogues (under similar polymerisation conditions with [Al$_{sMAO}$]$_0$/[Zr]$_0$ = 300); activities of 858 and 870 kg$_{PE}$ mol$_M^{-1}$ h^{-1} bar^{-1} at 60 °C for ***rac*-3**$_{sMAO}$ and sMAO-*rac*-($^{3\text{-Me}}$Ind$^{\#}$)$_2$ZrCl$_2$ respectively, and activities of 864 and 1063 kg$_{PE}$ mol$_M^{-1}$ h^{-1} bar^{-1} at 60 °C for ***rac*-4**$_{sMAO}$ and sMAO-*rac*-($^{3\text{-Me}}$Ind$^{\#}$)$_2$Zr(CH$_2$Ph)$_2$ respectively.[35] However, ***meso*-3**$_{sMAO}$ shows polymerisation activities approximately double sMAO-*meso*-($^{3\text{-Me}}$Ind$^{\#}$)$_2$ZrCl$_2$ (651 and 343 kg$_{PE}$ mol$_M^{-1}$ h^{-1} bar^{-1} respectively at 60 °C).[35]

Looking at the *meso*-catalysts, below 70 °C polymerisation activity follows the order ***meso*-4**$_{sMAO}$, ***meso*-3**$_{sMAO}$, and ***meso*-2**$_{sMAO}$ (activities of 657, 561, and 452 kg$_{PE}$ mol$_M^{-1}$ h^{-1} bar^{-1}, respectively). This is likely due to faster formation of the active species, as catalysts containing halide initiation groups first need to be alkylated.[36,37] ***meso*-4**$_{sMAO}$ shows less resilience to higher polymerisation temperatures and, as a result, the polymerisation activities converge to approximately 250 kg$_{PE}$ mol$_M^{-1}$ h^{-1} bar^{-1} at 90 °C.

Reducing the steric bulk in the indenyl ligand leads to increases in polymerisation activities; the 3-methyl catalyst ***meso*-5**$_{sMAO}$ shows higher polymerisation activities than the corresponding 3-ethyl catalyst ***meso*-2**$_{sMAO}$ (maximum activities of 927 kg$_{PE}$ mol$_M^{-1}$ h^{-1} bar^{-1} at 70 °C and 503 kg$_{PE}$ mol$_M^{-1}$ h^{-1} bar^{-1} at 50 °C, respectively). Unlike the other catalysts, which show continual decreases in activity with increasing temperature, ***meso*-5**$_{sMAO}$ shows a peak in activity at 70 °C (927 kg$_{PE}$ mol$_M^{-1}$ h^{-1} bar^{-1}) which could be related to the fact that ***meso*-5**$_{sMAO}$ possesses the largest gap aperture (α = 54.35(13)°).[38,39] ***meso*-5**$_{sMAO}$ displays lower polymerisation activity than the ethylene bridged analogue sMAO-*meso*-(EBI*)ZrCl$_2$; activities of 874 and 1331 kg$_{PE}$ mol$_M^{-1}$ h^{-1} bar^{-1} respectively at 60 °C (under similar polymerisation conditions with [Al]$_0$/[Zr]$_0$ = 300),[35] and lower than solution phase of well-known metallocene complexes.[40]

The molecular weights (M_w) and molecular weights distribution (M_w/M_n) of the polyethylenes produced were analysed by gel permeation chromatography (GPC) (Fig. 3). ***rac*-3**$_{sMAO}$ and ***rac*-4**$_{sMAO}$ produce polymers with similar molecular weights; 391 and 381 kg mol^{-1} at 50 °C, which is expected due to their similar polymerisation activities. ***rac*-3**$_{sMAO}$ produces polymers with lower molecular weights than the dimethyl silyl bridged analog, M_w of 447 mol^{-1} at 50 °C for sMAO-*rac*-^{Me_2}SB($^{3\text{-Et}}$I*)

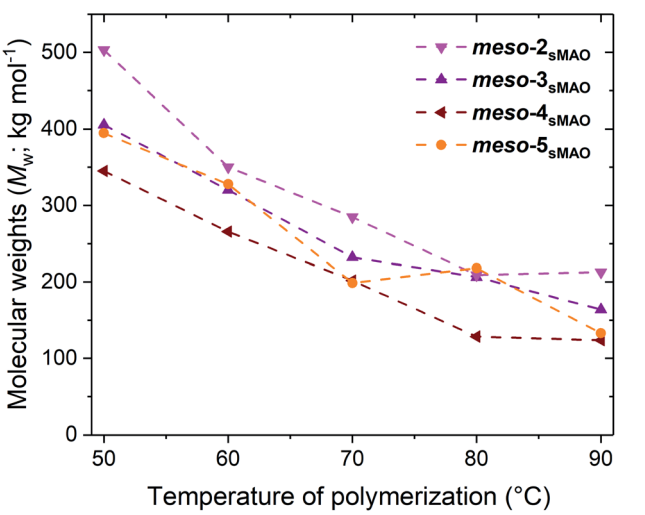

Fig. 3 Molecular weights (M_w) as a function of temperature of polymerisation using sMAO supported *meso*-($^{3\text{-Et}}$Ind$^{\#}$)$_2$ZrBr$_2$ (***meso*-2**$_{sMAO}$; pink down triangle), *meso*-($^{3\text{-Et}}$Ind$^{\#}$)$_2$ZrCl$_2$ (***meso*-3**$_{sMAO}$; purple triangle), *meso*-($^{3\text{-Et}}$Ind$^{\#}$)$_2$Zr(CH$_2$Ph)$_2$ (***meso*-4**$_{sMAO}$; brown right triangle), and *meso*-($^{3\text{-Me}}$Ind$^{\#}$)$_2$ZrBr$_2$ (***meso*-5**$_{sMAO}$; orange hexagon). Polymerisation conditions: ethylene (2 bar), pre-catalyst (10 mg), hexane (50 mL), [Al$_{sMAO}$]$_0$/[M]$_0$ = 200, TiBA (1000 eq.), and 30 minutes.

$ZrCl_2$. ***rac*-3-Hf$_{sMAO}$** produced polymers with the lowest molecular weights (297 kg mol^{-1} at 50 °C). For the *meso*-3-ethyl catalysts, ***meso*-2$_{sMAO}$** produced polymers with the highest molecular weights, followed by ***meso*-3$_{sMAO}$** and ***meso*-4$_{sMAO}$** (M_w of 503, 406, and 345 kg mol^{-1}, respectively, at 50 °C). ***meso*-5$_{sMAO}$** produced polymers with almost identical molecular weights to ***meso*-3$_{sMAO}$** (395 kg mol^{-1} at 50 °C). All polymers show the expected decreases in polymer molecular weights with increasing polymerisation temperature, attributed to stronger chain transfer reactions at elevated temperatures.[41] No long chain branching was observed by GPC or NMR spectroscopy,[42,43] but very large molecular weights distribution were observed (M_w/M_n around 5–8, Tables S4–S9†) which will point towards several catalytic species on the surface.[44]

Conclusions

A new family of unbridged bis(peralkylindenyl) zirconocene complexes of the type $(^{3\text{-R}}\text{Ind}^{\#})_2ZrX_2$ have been synthesised and fully characterised. Six new crystal structures have been reported.

When immobilised on solid polymethylaluminoxane (sMAO) these complexes produce HDPE in slurry-phase ethylene polymerisations. The supported *meso*-alkyl catalysts showing higher polymerisation activities than *meso*-halide catalysts; polymerisation activity follows the order ***meso*-4$_{sMAO}$**, ***meso*-3$_{sMAO}$**, and ***meso*-2$_{sMAO}$**.

These metallocene complexes and their inorganic based supported catalysts show promising results for use as slurry-phase polymerisation catalysts. Further testing with hydrogen, co-monomers and α-olefins will be carried out.

Experimental section

General details, synthesis and characterisation of ligands precursors, NMR spectra, X-ray crystallography data and further polymerisation data are included in the ESI.†

Synthesis of $(^{3\text{-Ph}}\text{Ind}^{\#})_2ZrCl_2$ (1)

2.0 equivalents $^{3\text{-Ph}}\text{Ind}^{\#}\text{Li}$ (2.00 g, 7.45 mmol) and 1.0 equivalent $ZrCl_4$ (0.868 g, 3.73 mmol) were stirred in benzene (100 mL) for 16 hours at room temperature. The reaction mixture was allowed to settle, filtered and the resulting orange filtrate dried *in vacuo* to afford a 50 : 50 mixture of *rac*-$(^{3\text{-Ph}}\text{Ind}^{\#})_2ZrCl_2$ (***rac*-1**) and *meso*-$(^{3\text{-Ph}}\text{Ind}^{\#})_2ZrCl_2$ (***meso*-1**) as an orange-yellow solid in 45% yield (1.15 g, 1.68 mmol). ^{1}H NMR (chloroform-d_1, 400 MHz, 298 K) δ (ppm): 7.75 (Ph-**H**, 2H, d, $^3J_{HH} = 7.5$ Hz), 7.56 (Ph-**H**, 2H, d, $^3J_{HH} = 7.5$ Hz), 7.28 (Ph-**H**, 4H, m), 7.18 (Ph-**H**, 6H, m), 7.14 (Ph-**H**, 2H, m), 6.91 (Ph-**H**, 2H, m), 6.88 (Ph-**H**, 2H, m), 6.42 (Ind-**H**, 2H, s), 5.76 (Ind-**H**, 2H, s), 2.63 (Ind-C**H$_3$**, 6H, s), 2.19 (Ind-C**H$_3$**, 6H, s), 2.17 (Ind-C**H$_3$**, 12H, s), 2.11 (Ind-C**H$_3$**, 12H, s), 2.08 (Ind-C**H$_3$**, 6H, s), 1.92 (Ind-C**H$_3$**, 6H, s), 1.88 (Ind-C**H$_3$**, 6H, s), 1.54 (Ind-C**H$_3$**, 6H, s). ^{13}C{^{1}H} NMR (chloroform-d_1, 101 MHz, 298 K) δ (ppm): 136.1 (Ind-**Ph**), 136.0 (Ind-**Ph**), 134.9 (**Ind**), 134.8 (**Ind**), 134.0 (**Ph**-H), 133.7 (**Ind**), 133.6 (**Ind**), 132.5 (**Ind**), 132.4 (**Ph**-H), 132.2 (**Ph**-H), 132.1 (**Ph**-H), 131.8 (**Ind**), 130.7 (**Ind**), 130.5 (**Ind**), 130.5 (**Ind**), 127.9 (**Ind**), 127.7 (**Ph**-H), 127.6 (**Ind**), 127.6 (**Ind**), 127.3 (**Ph**-H), 127.3 (**Ph**-H), 127.1 (**Ph**-H), 127.0 (**Ph**-H), 127.0 (**Ph**-H), 125.8 (**Ind**), 125.4 (**Ind**), 125.1 (**Ind**), 124.4 (**Ind**), 98.6 (**Ind**-H), 94.4 (**Ind**-H), 18.8 (Ind-**C**H$_3$), 18.5 (Ind-**C**H$_3$), 18.3 (Ind-**C**H$_3$), 17.1 (Ind-**C**H$_3$), 16.9 (Ind-**C**H$_3$), 16.8 (Ind-**C**H$_3$), 16.7 (Ind-**C**H$_3$), 16.7 (Ind-**C**H$_3$), 16.6 (Ind-**C**H$_3$), 15.1 (Ind-**C**H$_3$). CHN analysis (%): calculated C 70.15, H 6.18; observed C 70.26, H 6.38. HRMS (ESI): expected *m*/*z* 682.1705; observed 682.1736 [M]$^+$.

Synthesis of $(^{3\text{-Et}}\text{Ind}^{\#})_2ZrBr_2$ (*meso*-2)

2.0 equivalents $^{3\text{-Et}}\text{Ind}^{\#}\text{Li}$ (2.00 g, 9.08 mmol) and 1.0 equivalent $ZrBr_4$ (1.87 g, 4.54 mmol) were stirred in benzene (100 mL) for 16 hours at room temperature. The reaction mixture was allowed to settle, filtered and the resulting orange filtrate dried *in vacuo* to afford a 40 : 60 mixture of *rac*-$(^{3\text{-Et}}\text{Ind}^{\#})_2ZrBr_2$ and *meso*-$(^{3\text{-Et}}\text{Ind}^{\#})_2ZrBr_2$ as an orange solid. Recrystallisation of the isomeric mixture in DCM at −30 °C yielded *meso*-$(^{3\text{-Et}}\text{Ind}^{\#})_2ZrBr^2$ (***meso*-2**) as orange crystals in 6% yield (0.178 g, 0.263 mmol). Orange crystals of *meso*-$(^{3\text{-Et}}\text{Ind}^{\#})_2ZrBr_2$ suitable for a single crystal X-ray diffraction study were grown in pentane at room temperature. *meso*-$(^{3\text{-Et}}\text{Ind}^{\#})_2ZrBr_2$: ^{1}H NMR (chloroform-$d_1$, 400 MHz, 298 K) δ (ppm): 6.25 (Ind-**H**, 2H, s), 3.22 (Ind-C**H$_2$**–CH$_3$, 2H, dq, $^2J_{HH} = 15.0$ Hz, $^3J_{HH} = 7.5$ Hz), 2.69 (Ind-C**H$_2$**–CH$_3$, 2H, dq, $^2J_{HH} = 15.0$ Hz, $^3J_{HH} = 7.5$ Hz), 2.54 (Ind-C**H$_3$**, 12H, s), 2.27 (Ind-C**H$_3$**, 6H, s), 2.23 (Ind-C**H$_3$**, 6H, s), 1.70 (Ind-C**H$_3$**, 6H, s), 1.05 (Ind-CH$_2$–C**H$_3$**, 6H, t, $^3J_{HH} = 7.5$ Hz). ^{13}C{^{1}H} NMR (chloroform-d_1, 101 MHz, 298 K) δ (ppm): 134.2 (**Ind**), 133.4 (**Ind**), 130.9 (**Ind**), 130.8 (**Ind**), 127.8 (**Ind**), 126.0 (**Ind**), 125.6 (**Ind**), 125.2 (**Ind**), 94.6 (**Ind**-H), 23.0 (Ind-**C**H$_2$–CH$_3$), 17.6 (Ind-**C**H$_3$), 17.1 (Ind-**C**H$_3$), 16.8 (Ind-**C**H$_3$), 16.6 (Ind-**C**H$_3$), 15.6 (Ind-CH$_2$–**C**H$_3$), 14.6 (Ind-**C**H$_3$). CHN analysis (%): calculated C 56.71, H 6.25; observed C 56.61, H 6.33. HRMS (ESI): expected *m*/*z* 674.0695; observed 674.0724 [M]$^+$.

Synthesis of *rac*-$(^{3\text{-Et}}\text{Ind}^{\#})_2Zr(CH_2Ph)_2$ (*rac*-4)

1.0 equivalent *rac*-$(^{3\text{-Et}}\text{Ind}^{\#})_2ZrCl_2$ (45.2 mg, 0.0768 mmol) and 2.0 equivalents KCH_2Ph (20.0 mg, 0.154 mmol) were stirred in benzene (1 mL) for 16 hours at room temperature. The reaction mixture was allowed to settle, filtered and the resulting yellow filtrate dried *in vacuo* to afford *rac*-$(^{3\text{-Et}}\text{Ind}^{\#})_2Zr(CH_2Ph)_2$ (***rac*-4**) as a yellow solid in 93% yield (50.2 mg, 0.0717 mmol). Yellow crystals of *rac*-$(^{3\text{-Et}}\text{Ind}^{\#})_2Zr(CH_2Ph)_2$ suitable for a single crystal X-ray diffraction study were grown in pentane at −30 °C. ^{1}H NMR (chloroform-d_1, 400 MHz, 298 K) δ (ppm): 7.08 (*m*-Ph-**H**, 4H, dd, $^3J_{HH} = 7.3$, 7.4 Hz), 6.80 (*p*-Ph-**H**, 2H, t, $^3J_{HH} = 7.3$ Hz), 6.62 (*o*-Ph-**H**, 4H, d, $^3J_{HH} = 7.4$ Hz), 4.91 (Ind-**H**, 2H, s), 2.76 (Ind-C**H$_2$**–CH$_3$, 2H, dq, $^2J_{HH} = 14.8$ Hz, $^3J_{HH} = 7.4$ Hz), 2.51 (Ind-C**H$_3$**, 6H, s), 2.45 (Ind-C**H$_2$**–CH$_3$, 2H, dq, $^2J_{HH} = 14.8$ Hz, $^3J_{HH} = 7.4$ Hz), 2.28 (Ind-C**H$_3$**, 6H, s), 2.23 (Ind-C**H$_3$**, 6H, s), 2.01 (Ind-C**H$_3$**, 6H, s), 1.82 (Ind-C**H$_3$**, 6H, s), 0.99 (Ind-CH$_2$–C**H$_3$**, 6H, t, $^3J_{HH} = 7.4$ Hz), 0.87 (Zr-C**H$_2$**-Ph, 2H, d, $^2J_{HH} = 11.2$ Hz), 0.67 (Zr-C**H$_2$**-Ph, 2H, d, $^2J_{HH} = 11.2$ Hz). ^{13}C{^{1}H} NMR (chloroform-d_1, 101 MHz, 298 K) δ (ppm): 152.8 (Zr–CH$_2$-**Ph**), 133.3 (**Ind**), 131.0 (**Ind**), 128.3 (**Ind**), 127.9 (**Ind**), 127.8 (**Ind**), 127.6 (*m*-**Ph**), 127.1 (*o*-**Ph**), 126.4 (**Ind**), 123.2 (**Ind**), 121.0 (*p*-**Ph**), 119.8 (**Ind**), 100.8 (**Ind**-H), 66.0 (Zr-**C**H$_2$-Ph), 21.6 (Ind-**C**H$_2$–CH$_3$), 17.1 (Ind-**C**H$_3$), 16.8

(Ind-CH_3), 16.7 (Ind-CH_3), 16.6 (Ind-CH_3), 16.0 (Ind-CH_2–CH_3), 13.1 (Ind-CH_3). CHN analysis (%): calculated C 78.91, H 8.06; observed C 78.91, H 8.15.

Synthesis of *meso*-($^{3\text{-Et}}$Ind$^{\#}$)$_2$Zr(CH_2Ph)$_2$ (*meso*-4)

1.0 equivalent *meso*-($^{3\text{-Et}}$Ind$^{\#}$)$_2$ZrCl_2 (45.2 mg, 0.0768 mmol) and 2.0 equivalents KCH_2Ph (20.0 mg, 0.154 mmol) were stirred in benzene (1 mL) for 16 hours at room temperature. The reaction mixture was allowed to settle, filtered, and the resulting yellow filtrate dried *in vacuo* to afford *meso*-($^{3\text{-Et}}$Ind$^{\#}$)$_2$Zr(CH_2Ph)$_2$ (***meso*-4**) as a yellow solid in 93% yield (49.9 mg, 0.0713 mmol). Orange crystals of *meso*-($^{3\text{-Et}}$Ind$^{\#}$)$_2$Zr(CH_2Ph)$_2$ suitable for a single crystal X-ray diffraction study were grown in pentane at −30 °C. ^{1}H NMR (chloroform-d_1, 400 MHz, 298 K) δ (ppm): 7.06 (*m*-Ph-**H**, 2H, dd, $^3J_{HH}$ = 7.3, 7.6 Hz), 7.04 (*m*-Ph-**H**, 2H, dd, $^3J_{HH}$ = 7.3, 7.6 Hz), 6.79 (*p*-Ph-**H**, 1H, t, $^3J_{HH}$ = 7.3 Hz), 6.75 (*p*-Ph-**H**, 1H, t, $^3J_{HH}$ = 7.3 Hz), 6.58 (*o*-Ph-**H**, 2H, d, $^3J_{HH}$ = 7.6 Hz), 6.46 (*o*-Ph-**H**, 2H, d, $^3J_{HH}$ = 7.6 Hz), 5.61 (Ind-**H**, 2H, s), 2.71 (Ind-C**H$_2$**–CH_3, 2H, dq, $^2J_{HH}$ = 14.8 Hz, $^3J_{HH}$ = 7.4 Hz), 2.45 (Ind-C**H$_3$**, 6H, s), 2.38 (Ind-C**H$_2$**–CH_3, 2H, dq, $^2J_{HH}$ = 14.8 Hz, $^3J_{HH}$ = 7.4 Hz), 2.22 (Ind-C**H$_3$**, 6H, s), 2.18 (Ind-C**H$_3$**, 6H, s), 2.10 (Ind-C**H$_3$**, 6H, s), 1.77 (Ind-C**H$_3$**, 6H, s), 0.95 (Ind-CH_2–C**H$_3$**, 6H, t, $^3J_{HH}$ = 7.4 Hz), 0.79 (Zr–C**H$_2$**-Ph, 2H, s), 0.24 (Zr–C**H$_2$**-Ph, 2H, s). ^{13}C{^{1}H} NMR (chloroform-d_1, 101 MHz, 298 K) δ (ppm): 153.8 (Zr–CH_2-**Ph**), 152.7 (Zr–CH_2-**Ph**), 133.1 (**Ind**), 131.8 (**Ind**), 127.6 (*m*-**Ph**), 127.5 (**Ind**), 127.5 (*m*-**Ph**), 127.3 (**Ind**), 127.2 (*o*-**Ph**), 126.9 (**Ind**), 126.6 (*o*-**Ph**), 126.5 (**Ind**), 123.3 (**Ind**), 121.1 (*p*-**Ph**), 120.7 (*p*-**Ph**), 118.9 (**Ind**), 100.7 (**Ind**-H), 67.5 (Zr-**C**H_2-Ph), 66.3 (Zr-**C**H_2-Ph), 22.0 (Ind-**C**H_2–CH_3), 17.1 (Ind-**C**H_3), 16.8 (Ind-**C**H_3), 16.7 (Ind-**C**H_3), 16.6 (Ind-**C**H_3), 16.2 (Ind-CH_2–**C**H_3), 13.1 (Ind-**C**H_3). CHN analysis (%): calculated C 78.91, H 8.06; observed C 78.79, H 8.16.

Synthesis of *meso*-($^{3\text{-Me}}$Ind$^{\#}$)$_2$ZrBr_2 (*meso*-5)

2.0 equivalents Ind$^{\#}$Li (2.00 g, 9.70 mmol) and 1.0 equivalent ZrBr_4 (1.99 g, 4.85 mmol) were stirred in benzene (100 mL) for 16 hours at room temperature. The reaction mixture was allowed to settle, filtered and the resulting red filtrate dried *in vacuo* to afford an orange solid comprising of a 20 : 80 mixture of *rac*-($^{3\text{-Me}}$Ind$^{\#}$)$_2$ZrBr_2 and *meso*-($^{3\text{-Me}}$Ind$^{\#}$)$_2$ZrBr_2 and impurities. Recrystallisation of the isomeric mixture in toluene at −30 °C yielded *meso*-($^{3\text{-Me}}$Ind$^{\#}$)$_2$ZrBr_2 (***meso*-5**) as orange crystals, suitable for a single crystal X-ray diffraction study, in 6% yield (0.180 g, 0.277 mmol). ^{1}H NMR (chloroform-d_1, 400 MHz, 298 K) δ (ppm): 5.90 (Ind-**H**, 2H, s), 2.64 (Ind-C**H$_3$**, 6H, s), 2.55 (Ind-C**H$_3$**, 6H, s), 2.22 (Ind-C**H$_3$**, 6H, s), 2.20 (Ind-C**H$_3$**, 6H, s), 2.17 (Ind-C**H$_3$**, 6H, s), 2.12 (Ind-C**H$_3$**, 6H, s). ^{13}C{^{1}H} NMR (chloroform-d_1, 101 MHz, 298 K) δ (ppm): 134.0 (**Ind**), 133.4 (**Ind**), 131.0 (**Ind**), 129.6 (**Ind**), 127.4 (**Ind**), 127.4 (**Ind**), 126.8 (**Ind**), 121.2 (**Ind**), 96.7 (**Ind**-H), 17.5 (Ind-**C**H_3), 16.7 (Ind-**C**H_3), 16.6 (Ind-**C**H_3), 16.6 (Ind-**C**H_3), 16.6 (Ind-**C**H_3), 16.2 (Ind-**C**H_3). CHN analysis (%): calculated C 55.46, H 5.90; observed C 55.50, H 6.02. HRMS (EI): expected *m*/*z* 646.0382; observed 646.0366 [M]$^+$.

Synthesis of *meso*-($^{3\text{-Me}}$Ind$^{\#}$)$_2$Zr(CH_2Ph)$_2$ (*meso*-6)

1.0 equivalent *meso*-(Ind$^{\#}$)$_2$ZrBr_2 (49.9 mg, 0.0768 mmol) and 2.0 equivalents KCH_2Ph (20.0 mg, 0.154 mmol) were stirred in benzene (1 mL) for 16 hours at room temperature. The reaction mixture was allowed to settle, filtered and the resulting yellow filtrate dried *in vacuo* to afford *meso*-($^{3\text{-Me}}$Ind$^{\#}$)$_2$Zr(CH_2Ph)$_2$ (***meso*-6**) as a yellow solid in 88% yield (45.6 mg, 0.0678 mmol). Yellow crystals of *meso*-($^{3\text{-Me}}$Ind$^{\#}$)$_2$Zr(CH_2Ph)$_2$ suitable for a single crystal X-ray diffraction study were grown in toluene at room temperature. ^{1}H NMR (chloroform-d_1, 500 MHz, 298 K) δ (ppm): 7.09 (*m*-Ph-**H**, 2H, dd, $^3J_{HH}$ = 7.3, 7.6 Hz), 7.04 (*m*-Ph-**H**, 2H, dd, $^3J_{HH}$ = 7.3, 7.6 Hz), 6.82 (*p*-Ph-**H**, 1H, t, $^3J_{HH}$ = 7.3 Hz), 6.76 (*p*-Ph-**H**, 1H, t, $^3J_{HH}$ = 7.3 Hz), 6.61 (*o*-Ph-**H**, 2H, d, $^3J_{HH}$ = 7.6 Hz), 6.48 (*o*-Ph-**H**, 2H, d, $^3J_{HH}$ = 7.6 Hz), 5.37 (Ind-**H**, 2H, s), 2.51 (Ind-C**H$_3$**, 6H, s), 2.22 (Ind-C**H$_3$**, 6H, s), 2.21 (Ind-C**H$_3$**, 6H, s), 2.18 (Ind-C**H$_3$**, 6H, s), 2.12 (Ind-C**H$_3$**, 6H, s), 1.71 (Ind-C**H$_3$**, 6H, s), 1.11 (Zr–C**H$_2$**-Ph, 2H, s), 0.31 (Zr–C**H$_2$**-Ph, 2H, s). ^{13}C{^{1}H} NMR (chloroform-d_1, 125 MHz, 298 K) δ (ppm): 152.9 (Zr–CH_2-**Ph**), 152.8 (Zr–CH_2-**Ph**), 132.9 (**Ind**), 131.5 (**Ind**), 128.0 (**Ind**), 127.9 (**Ind**), 127.7 (*m*-**Ph**), 127.5 (*m*-**Ph**), 127.4 (**Ind**), 127.1 (*o*-**Ph**), 126.8 (*o*-**Ph**), 126.3 (**Ind**), 125.1 (**Ind**), 121.1 (*p*-**Ph**), 120.7 (*p*-**Ph**), 113.6 (**Ind**), 100.1 (**Ind**-H), 67.6 (Zr-**C**H_2-Ph), 66.8 (Zr-**C**H_2-Ph), 17.6 (Ind-**C**H_3), 16.9 (Ind-**C**H_3), 16.6 (Ind-**C**H_3), 16.5 (Ind-**C**H_3), 14.9 (Ind-**C**H_3), 13.5 (Ind-**C**H_3).

Synthesis of sMAO supported metallocene catalysts

200 equivalents sMAO (39.7 or 41.1% wt$_{Al}$; 0.300 g, 4.41 or 4.57 mmol$_{Al}$) were dispersed in toluene (25 mL) to form a colourless slurry. 1.0 equivalent of a metallocene complex (0.0221 or 0.0229 mmol) was dissolved in toluene (25 mL) to form a colored solution which was then quickly added to the sMAO at room temperature. A mixture of *rac*- and *meso*-isomer of the complex, and the Al : complex molar ratio of 200 : 1 were used unless stated otherwise. The reaction mixture was heated to 60 °C for 2 hours with occasional swirling. The coloured solid was allowed to settle from the clear, colourless solution which was decanted, and the solid was dried *in vacuo* to afford the product as follows:

Ethylene polymerisation

A supported metallocene catalyst (10.0 mg, 1.0 eq$_{complex}$), TiBA (1000 eq.) and hexane (50 mL) were added to a 150 mL Rotaflo ampoule containing a stirrer bar. The ampoule was sealed and degassed before being heated to the desired temperature at the stirring speed of 1000 rpm. The ampoule was then opened to ethylene (2 bar). On completion of the test, the ampoule was closed to ethylene and degassed. The resulting polyethylene was filtered on a glass sintered frit, washed with pentane (2 × 25 mL) and dried. All polymerisation tests were carried out, at least, in duplicate and run for 30 minutes, unless stated otherwise, or until the stirring ceased entirely. The activities were reported as an average with ±1 ESD error. The molecular weights (M_w) of the resulting polyethylenes were determined by GPC and reported with their corresponding molecular weight distribution (M_w/M_n) values.

Conflicts of interest

There are no conflicts to declare.

Acknowledgements

P. A., J. V. L., J.-C. B., and Z. R. T. (SCG Research Fellowship) would like to thank SCG Chemicals Co., Ltd (Thailand) for financial support; Chemical Crystallography (University of Oxford) for the use of the diffractometers; and Ms Liv Thobru (Norner AS, Norway) for GPC analysis.

Notes and references

1 L. Resconi, L. Cavallo, A. Fait and F. Piemontesi, *Chem. Rev.*, 2000, **100**, 1253–1346.
2 W. Kaminsky and H. Sinn, *Adv. Polym. Sci.*, 2013, **258**, 1–28; *Methylaluminoxane: Key Component for New Polymerization Catalysts*, ed. W. Kaminsky, Springer. Polyolefins: 50 years after Ziegler and Natta II.
3 N. Schneider, M. E. Huttenloch, U. Stehling, R. Kirsten, F. Schaper and H. H. Brintzinger, *Organometallics*, 1997, **16**, 3413–3420.
4 M. Bochmann, *J. Chem. Soc. Dalton Trans.*, 1996, 255–270.
5 G. G. Hlatky, *Chem. Rev.*, 2000, **100**, 1347–1376.
6 B. Wang, *Coord. Chem. Rev.*, 2006, **250**, 242–258.
7 O. Olabisi, M. Atiqullah and W. Kaminsky, *J. Macromol. Sci., Part C*, 1997, **37**, 519–554.
8 W. Kaminsky and H. Winkelbach, *Top. Catal.*, 1999, **7**, 61–67.
9 W. Kaminsky, *Catal. Today*, 1994, **20**, 257–271.
10 W. Kaminsky, *J. Chem. Soc., Dalton Trans.*, 1998, 1413–1418.
11 W. Kaminsky, *Adv. Catal.*, 2001, **46**, 89–159.
12 W. Kaminsky and A. Laban, *Appl. Catal., A*, 2001, **222**, 47–61.
13 W. Kaminsky, *J. Polym. Sci., Polym. Chem.*, 2004, **42**, 3911–3921.
14 W. Kaminsky, A. Funck and H. Hähnsen, *Dalton Trans.*, 2009, 8803–8810.
15 H. G. Alt, *Dalton Trans.*, 2005, 3271–3276.
16 W. Kaminsky, *Macromol. Symp.*, 1995, **97**, 79–89.
17 C. Janiak and B. Rieger, *Angew. Chem.*, 1994, **215**, 47–57.
18 P. A. Zapata, C. Belver, R. Quijada, P. Aranda and E. Ruiz-Hitzky, *App. Catal. A Gen.*, 2013, **453**, 142–150.
19 D. Bianchini, J. H. Z. dos Santos, T. Uozumi and T. Sano, *J. Mol. Catal. A: Chem.*, 2002, **185**, 223–235.
20 C. Janiak, B. Rieger, R. Voelkel and H.-G. Braun, *J. Polym. Sci., Polym. Chem.*, 1993, **31**, 2959–2968.
21 H. Cramail, K. Radhakrishnan and A. Deffieux, *Compt. Rend.*, 2002, **5**, 49–52.
22 T. Dalet, H. Cramail and A. Deffieux, *Macromol. Chem. and Phys.*, 2004, **205**, 1394–1401.
23 M. M. Mortazavi, S. Ahmadjo, J. H. Z. Dos Santos, H. Arabi, M. Nekoomanesh, G. H. Zohuri, R. Brambilla and G. B. Galland, *J. Appl. Polym. Sci.*, 2013, **130**, 4568–4575.
24 F. Silveira, M. D. C. Martins Alves, F. C. Stedile, S. B. Pergher and J. H. Z. dos Santos, *J. Mol. Catal. A Chem.*, 2010, **315**, 213–220.
25 J.-C. Buffet, Z. R. Turner, R. T. Cooper and D. O'Hare, *Polym. Chem.*, 2015, **6**, 2493–2503.
26 J.-C. Buffet, N. Wanna, T. A. Q. Arnold, E. K. Gibson, P. P. Wells, Q. Wang, J. Tantirungrotechai and D. O'Hare, *Chem. Mater.*, 2015, **27**, 1495–1501.
27 J. C. Buffet, C. F. H. Byles, R. Felton, C. P. Chen and D. O'Hare, *Chem. Commun.*, 2016, **52**, 4076–4079.
28 A. F. R. Kilpatrick, J.-C. Buffet, P. Nørby, N. H. Rees, N. P. Funnell, S. Sripothongnak and D. O'Hare, *Chem. Mater.*, 2016, **28**, 7444–7450.
29 A. F. R. Kilpatrick, N. H. Rees, S. Sripothongnak, J.-C. Buffet and D. O'Hare, *Organometallics*, 2018, **37**, 156–164.
30 P. Angpanitcharoen, G. Hay, J.-C. Buffet, Z. R. Turner, T. A. Q. Arnold and D. O'Hare, *Polyhedron*, 2016, **116**, 216–222.
31 P. Angpanitcharoen, J. V. Lamb, Z. R. Turner, J.-C. Buffet and D. O'Hare, *Mol. Catal.*, 2020, **498**, 111275.
32 T. A. Q. Arnold, J.-C. Buffet, Z. R. Turner and D. O'Hare, *J. Organomet. Chem.*, 2015, **792**, 55–65.
33 N. E. Grimmer, N. J. Coville, C. B. de Koning, J. M. Smith and L. M. Cook, *J. Organomet. Chem.*, 2000, **616**, 112–127.
34 N. Piccolrovazzi, P. Pino, G. Consiglio, A. Sironi and M. Moret, *Organometallics*, 1990, **9**, 3098–3105.
35 T. A. Q. Arnold, Z. R. Turner, J.-C. Buffet and D. O'Hare, *J. Organomet. Chem.*, 2016, **822**, 85–90.
36 T. K. Trefz, M. A. Henderson, M. Linnolahti, S. Collins and J. S. McIndoe, *Chem. -Eur. J.*, 2015, **21**, 2980–2991.
37 S. Collins, M. Linnolahti, M. G. Zamora, H. S. Zijlstra, M. T. Rodríguez Hernández and O. Perez-Camacho, *Macromolecules*, 2017, **50**, 8871–8884.
38 C. Janiak, K. C. H. Lange, U. Versteeg, D. Lentz and P. H. M. Budzelaar, *Chem. Ber.*, 1996, **129**, 1517–1529.
39 C. Janiak, U. versteeg, K. C. H. Lange, R. Weimann and E. Hahn, *J. Organomet. Chem.*, 1995, **501**, 219–234.
40 W. Kaminsky, R. Engehausen, K. Zoumis, W. Spaleck and J. Rohrmann, *Makromol. Chem.*, 1992, **193**, 1643–1651.
41 M. A. Parvez, M. Rahaman, M. A. Suleiman, J. B. P. Soares and I. A. Hussein, *Int. J. Polym. Sci.*, 2014, 1–10.
42 A. Malmberg, J. Liimatta, A. Lehtinen and B. Löfgren, *Macromolecules*, 1999, **32**, 6687–6696.
43 M. Pollard, K. Klimke, R. Graf, H. W. Spiess, M. Wilhelm, O. Sperber, C. Piel and W. Kaminsky, *Macromolecules*, 2004, **37**, 813–825.
44 A. Ahlers and W. Kaminsky, *Makromol. Chemie., Rapid. Commun.*, 1988, **9**, 457–461.